NASA Technical Memorandum 109031

ISAC: A TOOL FOR AEROSERVOELASTIC MODELING AND ANALYSIS

William M. Adams, Jr. and Sherwood Tiffany Hoadley

December 1993

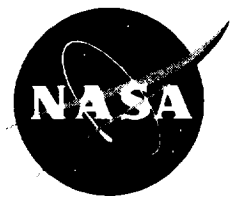

National Aeronautics and
Space Administration

Langley Research Center
Hampton, Virginia 23681-0001

ISAC: A TOOL FOR AEROSERVOELASTIC MODELING AND ANALYSIS

By William M. Adams, Jr.* and Sherwood Tiffany Hoadley**
NASA Langley Research Center, Hampton, Virginia 23681-0001

Abstract

This paper discusses the capabilities of the Interaction of Structures, Aerodynamics, and Controls (ISAC) system of program modules. The major modeling, analysis, and data management components of ISAC are identified. Equations of motion are displayed for a Laplace-domain representation of the unsteady aerodynamic forces. Options for approximating a frequency-domain ($i\omega$) representation of unsteady aerodynamic forces with rational functions of the Laplace variable (s) are shown. Linear time invariant state-space equations of motion that result are discussed. Model generation and analyses of stability and dynamic response characteristics are shown for an aeroelastic vehicle which illustrate some of the capabilities of ISAC as a modeling and analysis tool for aeroelastic applications.

Introduction

The goal of developing more profitable transport aircraft tends to result in more flexible and less inherently stable vehicles. The additional flexibility increases the likelihood of the need for active flutter suppression and gust and maneuver load alleviation. The lessened inherent stability results in the need for higher gain and, therefore, higher bandwidth "rigid mode" control. Both effects reduce the frequency separation between rigid and elastic modes. The desire for less observable, more agile fighters possessing good maneuvering capability over a large range of flight conditions leads to a need for similar analysis capabilities. Consequently, it is essential to have tools that consider the interactions that may arise between flexible structures, unsteady aerodynamics, and active controls.

During the early 1970's, the NASA Langley Research Center did not have access to an analysis tool to investigate such interactions. The Interaction of Structures, Aerodynamics, and Controls (ISAC) system of program modules was developed during the 1970's to provide the missing analysis capability[1] and continues to be an effective tool. Enhancements and refinements have been made during the 1980's.[2,3,4,5] Other aeroelastic packages containing similar analysis capabilities have been described in the literature. They include FLEXSTAB,[6] NASTRAN,[7] DYLOFLEX,[8] ADAM,[9] STARS,[10] and several industry-developed, proprietary codes.

This paper describes and illustrates the application of the ISAC system of program modules. ISAC provides an integrated assembly of linear techniques for modeling, data management, and analysis of actively controlled aeroelastic vehicles. Typical applications of ISAC include: generation of sensor output equations and rational function approximations of unsteady aerodynamic data for use in support of simulations of aircraft; development of reduced order design plant models for use in control law synthesis; evaluation of the performance of candidate control laws; as well as evaluation of the aeroelastic behavior of the open-loop vehicle.

ISAC is operable in either a batch or an interactive mode and provides a variety of selectable graphical outputs with which to track model generation and assess dynamic behavior. Results are shown that were obtained by using ISAC to model and analyze a flexible, research vehicle. The results herein and those of the references document many of the modeling and analysis options provided by ISAC.

Equations of Motion

Figure 1 illustrates the fact that ISAC expresses aircraft motion as perturbations from steady-state conditions in terms of a superposition of characteristic mode shapes (including rigid body modes when appropriate). Bold symbols in the figures and text refer to matrix or vector quantities. Variables shown in figure 1 are the generalized coordinates (ξ), displacement at a point (x, y) of a modeshape (Z_i), and displacement (z) at a point (x, y) due to a superposition of modeshapes. The modal characteristics, planform geometry, and flight conditions of interest are the basic inputs required by ISAC to initiate the development of aeroelastic models.

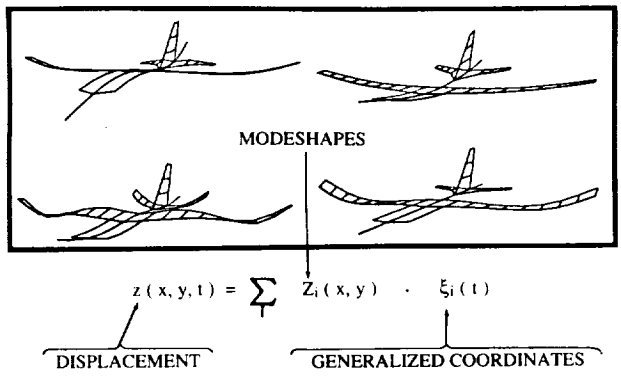

Fig. 1 Displacement as superposition of modeshapes.

The primary dynamic blocks that are included in ISAC in the development of a closed-loop mathematical model are shown in figure 2. They are: flexible aircraft (an externally provided modal characterization of the flexible aircraft that is typically, but not necessarily, in terms of an orthogonal set of *in vacuo* modes); aerodynamics (generalized unsteady aerodynamic forces which are Mach number and frequency dependent); sensor; controller; actuator; and gust spectra dynamic characteristics. The variable, η, represents statistically independent white noise inputs which, when passed through the gust filter, produce gust incidence angles, α_g, whose output power spectral densities correspond with user-defined gust spectra. Other, not previously defined, variables in figure 2 are the control surface deflections (δ), the commands to the actuators ($\mathbf{u}$), an external vector of commands ($\mathbf{u}_{com}$), and a vector of outputs ($\mathbf{y}$).

* Senior Research Engineer, 6 N. Dryden Street, MS 489.

** Senior Research Engineer, 647 Andrews Street, MS 340.

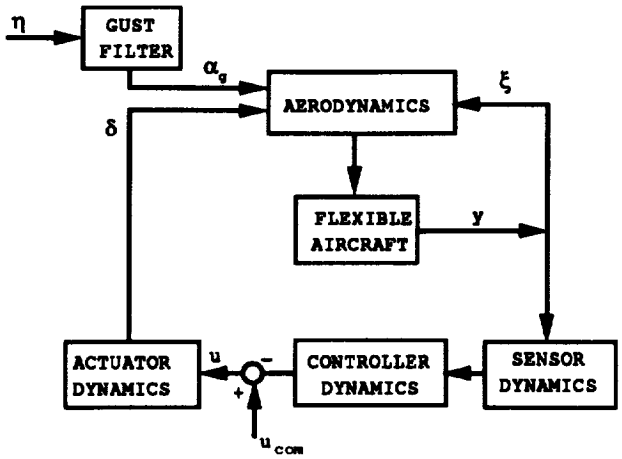

Fig. 2 Dynamic elements included in equations of motion.

Laplace-Domain Form

The Laplace-domain form of the plant equations of motion that are implemented in ISAC for an inertial, flutter-axis coordinate system and rectilinear motion are shown in equations (1) and (2).

$$\begin{bmatrix} G_{\xi\xi}(s) & G_{\xi\delta}(s) \\ 0 & I \end{bmatrix} \begin{pmatrix} \xi \\ \delta \end{pmatrix} = \begin{bmatrix} qQ_{\xi g}(s) & 0 \\ 0 & T_\delta(s) \end{bmatrix} \begin{pmatrix} \alpha_g \\ u \end{pmatrix} \qquad (1)$$

where

$$G_{\xi\xi} = M_{\xi\xi}\, s^2 + \begin{bmatrix} \ddots & 0 \\ & g_{\xi_i}(s)\, k_{\xi_i\xi_i} \\ 0 & \ddots \end{bmatrix} + K_{\xi\xi} - qQ_{\xi\xi} ,$$

and

$$G_{\xi\delta} = M_{\xi\delta}\, s^2 - qQ_{\xi\delta} ,$$

and

$$\begin{aligned} y &= T_S(s)\, \mathcal{C}(s)\, \mathcal{V} \\ &= T_S(s)\, [\mathcal{C}_\xi(s)\, \xi + \mathcal{C}_\delta(s)\, \delta + \mathcal{C}_g(s)\, \alpha_g]. \end{aligned} \qquad (2)$$

Here $\mathcal{C}(s)$ and $\mathcal{V}$ are defined in terms of their components, s refers to the Laplace variable, and the subscript g refers to gust inputs. The variable $Q = Q(N_{MA}, sb/V)$ refers to generalized aerodynamic forces arising from motion of the generalized coordinates, control surface deflections, and gust velocity inputs. The variable, N_{MA}, is Mach number, V is free stream airspeed, and b is a reference length, typically the mean aerodynamic semichord. The generalized mass ($M_{\xi\xi}$, $M_{\xi\delta}$), generalized stiffness, $K_{\xi\xi}$, and modeshape information, together with the model for structural damping defined below, define the modal characterization of the structure. The symbol $k_{\xi_i\xi_i}$ refers to the i^{th} diagonal element of $K_{\xi\xi}$. Up to three choices can be made by the user for the variable $g_{\xi_i}(s)$:

(a) $g_{\xi_i}(s) = \sqrt{-1}\, g_{si}$, the usual structural damping

(b) $g_{\xi_i}(s) = \frac{s}{|s|}\, g_{si}$, reduces to (a) for $s = i\omega$, or

(c) $g_{\xi_i}(s) = g_{si}\, \frac{s}{\omega_{n_i}}$, the usual viscous damping form when the stiffness matrix is diagonal ($m_{\xi_i\xi_i}\omega_{n_i}^2 = k_{\xi_i\xi_i}$ and $g_{\xi_i}(s) = 0$ if $\omega_{n_i} = 0$).

The variable, g_{si}, is a structural damping coefficient. Only the third form is allowed in the state-space formulation below.

$T_\delta(s)$ is a diagonal matrix of actuator transfer function dynamics, and q is dynamic pressure. $T_S(s)$, the sensor dynamics matrix, is also diagonal. The elements of $\mathcal{C}(s)$ in equation (2) are the contributions to the output y per unit generalized coordinate displacements, control deflections, and incremental incidence angles due to turbulence. Coordinate system options which admit analyses of perturbations from nonrectilinear flight conditions are also selectable in ISAC.

Closed-loop analyses are accomplished by replacing u with the following equation

$$u = -T_C(s)\, P_{Cy}\, y + u_{com} \qquad (3)$$

where P_{Cy} is a rectangular matrix of ones and zeros that selects a subset of the available outputs for feedback, $T_C(s)$ is a transfer matrix representation of a multi-input/multi-output controller, and u_{com} is a vector of external commands to the actuators.

The discussion thus far has assumed the availability of unsteady aerodynamic data in the complex s-plane. The aerodynamic data is typically only available on the imaginary axis at a finite number of frequencies. Nevertheless, with the Laplace-domain form of the equations and the approximation that $Q(s) \approx Q(0 + i\omega b/V)$ for lightly damped systems, commonly referred to as the p-k approximation,[11] stability analyses for open- and closed-loop systems can be performed using determinant or matrix iteration.[3,7,11] Frequency-domain analyses can also be performed to exhibit frequency responses and (for stable systems) power spectral densities and rms results for outputs of interest. Time-domain analyses can be performed using fast Fourier transform (FFT) techniques.[12] Results illustrating these capabilities will be shown below.

Linear Time Invariant State-Space Form

ISAC also provides the capability of converting the equations to a first order linear time invariant (LTI) state-space form with subsequent stability analyses performed using efficient, linear algebra techniques. This conversion is accomplished by approximating the frequency-dependent unsteady aerodynamic forces that are defined for a set of points on the s-plane imaginary axis with rational functions in s, the Laplace variable.[5,13,14,15,16,17] Two rational function approximation options available within ISAC to use in making the conversion to LTI state-space equations are shown in equations (4) and (5):

$$\hat{Q} = A_0 + A_1 \frac{sb}{V} + A_2 \left(\frac{sb}{V}\right)^2 + \sum_{j=1}^{\ell_1} A_{2+j}\, \frac{s}{s + \frac{V\beta_j}{b}} \qquad (4)$$

or, for R diagonal, positive definite, and $\ell_2 \times \ell_2$,

$$\hat{Q} = A_0 + A_1 \frac{sb}{V} + A_2 \left(\frac{sb}{V}\right)^2 + \tilde{D}\left[\frac{sb}{V} I - R\right]^{-1} \tilde{E}. \qquad (5)$$

In these equations, the matrix approximate, $\hat{Q}$, is $n_\xi \times (n_\xi + n_\delta + n_g)$; and ℓ_1 and ℓ_2 are the number of unique denominator poles in each type of approximation, respectively. The A_i, $\tilde{D}$, R and $\tilde{E}$ are real, constant matrices, and each $(-V\beta_j/b)$ is a stable, real denominator pole. The matrices $\tilde{D}$ and $\tilde{E}$ are of rank ℓ_2 for the usual case where $n_\xi > \ell_2$.

The Roger's[13] form, equation (4), allows rapid solution for the coefficient matrices that best fit the tabular data in a least squares sense, particularly if the denominator coefficients are chosen a priori rather than by optimization of a performance measure. However, the dimension of the added states corresponding to the rational approximation can be large, being equal to the product $(n_\xi \times \ell_1)$.

In the minimum-state approach[16] (equation (5)), because the matrices $\tilde{D}$ $(n_\xi \times \ell_2)$ and $\tilde{E}$ $(\ell_2 \times (n_\xi + n_\delta + n_g))$ are of rank ℓ_2, only ℓ_2 added states are required, independent of the number of generalized coordinates. Therefore, the minimum-state approach can offer a significant savings in number of added states with little or no penalty in accuracy of modeling the aerodynamic forces. However, solution for the coefficient matrices is time intensive requiring an iterative, two-step process.

A third option, not explicitly presented here but available in ISAC, allows a columnwise fit[5,17] of the form of equation (4). Each column can then have a different number of lag terms with different values for the denominator poles. A discussion of the advantages and disadvantages of these options is given in reference 5. Reference 15 discusses an approach, not currently implemented in ISAC, which, given the characteristic poles of the system for a specific flight condition, allows the rational portion of the unsteady aerodynamic forces to be modeled with no added state penalty.

These approximations, together with rational representations of sensor, actuator and gust spectra dynamics, allow a state-space model of the aeroelastic vehicle to be generated of the form shown in equations (6) and (7).

$$\dot{x} = Ax + B_u u + B_g \eta, \tag{6}$$

and

$$y = Cx + D_u u + D_g \eta. \tag{7}$$

See the appendix for more detail. The state vector is

$$x^T = (\xi^T, \dot{\xi}^T, x_a^T, x_S^T, x_A^T, x_g^T).$$

The subscripts a, S, A, and g refer to states due the rational function approximations, sensor dynamics, actuator dynamics and the gust filter dynamics, respectively.

The D_u and D_g can arise because of the rational function approximations. Consider the case of an accelerometer with negligible dynamics in the frequency range of interest. If $s^2T_{\delta j}$ is strictly proper (that is, the numerator is of lessor degree than the denominator) for each of the actuators, then D_u will be zero. If this condition is violated for the jth actuator, a nonzero D_u can be avoided by constraining to zero that column of A_2 (see eqs. (4) and (5)) which would make $s^2T_{\delta j}$ not strictly proper. Once a choice is made for gust spectra dynamics, similar considerations would be necessary to avoid the presence of D_g in an accelerometer output.

Once the state-space form is generated, it, or a reduced order approximation thereof, can be used as a design model of the plant to perform controller synthesis studies using state-space design techniques. Alternatively, tabular frequency-response representations developed without the need for the s-plane approximations can be used as design models for frequency-domain-based design techniques.[18]

Closed-loop analyses with the state-space representation can be accomplished by direct state-space definition of the controller or by converting a transfer-matrix controller representation to a state-space equivalent. The direct state-space controller is assumed to be of the form

$$\dot{x}_C = A_C x_C + B_C P_{Cy} y, \tag{8}$$

and

$$u = -(C_C x_C + D_C P_{Cy} y) + u_{com}, \tag{9}$$

where the subscript C refers to the controller. The matrix P_{Cy} selects a subset of the available outputs to use as feedback.

Major ISAC Components

The major ISAC components and their data communication links via the data complex are identified in figure 3; the figure also shows how ISAC outputs can provide aeroelastic design models for control law synthesis.

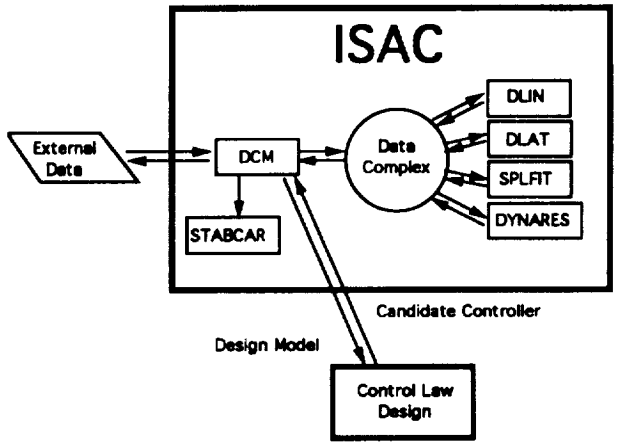

Fig. 3 Major modules contained in ISAC.

Data Storage and Management

The model development process is initiated by receipt and storage on the data complex of modal data from an external source. The data complex manager (DCM) facilitates this task and queries the user for dimensional and format characteristics of the data. The DCM catalogs the data with a user-provided descriptor and adds dimensional descriptors together with the time of storage. The DCM and the data complex are vital parts of the ISAC system of modules. The data complex is a random access storage facility for binary data. The data stored can include thirteen different types of data that represent not only information required to perform the aeroelastic modeling but also the state-space quadruples for each model that results. A single data complex may contain up to 100 separate data sets, each of which may contain all thirteen data types. Inputs made by the user direct the various ISAC modules as to where to store data received/created and how to uniquely identify that data for subsequent use. In addition, the DCM provides a user friendly interface allowing direct interactive access to the data complex contents.

Unsteady Aerodynamic Force Computations

The two modules DLIN and DLAT generate the basic information required to include unsteady aerodynamic forces

in the mathematical models. DLIN is a modal interpolation preprocessor for the DLAT module; and DLAT calculates unsteady aerodynamic forces using a doublet lattice[19] method. Alternatively, one or both of these modules could be bypassed if the data they generate were available from an external source. Once the aerodynamic description is complete, model generation at flight conditions of interest can be accomplished to provide design models or to perform analyses of stability and dynamic response characteristics.

The DLIN module accepts modeshape data from the data complex or from an external source together with information related to that data such as the number of structural sections and whether each structural section corresponds to a plate or a beam representation. A spline fit is made of the modeshape data. The next step is to utilize aerodynamic paneling inputs to determine the points at which interpolation is needed to obtain modal deflections and/or slopes. The interpolations are performed and the resulting data are stored on the data complex for subsequent use by the DLAT module in computing generalized aerodynamic forces.

The DLAT module is employed to compute unsteady aerodynamic force data for a specified Mach number and for a specified set of reduced (nondimensional) frequencies. The aerodynamic force data can be computed and saved on the data complex in two forms, $Q_{AIC}(N_{MA}, i\omega b/V)$ and $Q(N_{MA}, i\omega b/V)$. The matrix of modeshape independent aerodynamic influence coefficients, $Q_{AIC}(N_{MA}, i\omega b/V)$, is of dimension $n_b \times n_b$, where n_b is the number of boxes in the aerodynamic paneling. The ijth element of the aerodynamic influence matrix contains the pressure at box i due to a normal component of motion of box j. The matrix of generalized aerodynamic forces, $Q(N_{MA}, i\omega b/V)$, is of dimension $n_\xi \times (n_\xi + n_s + n_g)$. The aerodynamic influence coefficient matrix, together with modal data (e. g., that provided by the DLIN module), can be used to compute generalized forces as shown in equation (10).

$$Q_{ij}(N_{MA}, \frac{i\omega b}{V}) = Z_i^T Q_{AIC}(N_{MA}, \frac{i\omega b}{V})\, w_j, \qquad (10)$$

where Q_{ij} is the contribution to the generalized aerodynamic force in the ith degree of freedom due to harmonic motion in the jth degree of freedom, Z_i is displacement in the ith mode at each box pressure point, and w_j is downwash at each box downwash point due to harmonic motion of the jth mode.

A selectable set of rigid body, gust, and control rotation modes are also available within the DLAT module and can be employed to obtain stability and control derivative information and/or to augment elastic mode information from other sources. The doublet lattice[19] procedure is an integral part of the DLAT module (Augmentation is planned to enable generation of piston theory aerodynamic forces within ISAC for high Mach number unsteady conditions).

Model Formation and Analysis

Components used to determine stability and response characteristics as well as to generate s-plane approximations of the unsteady aerodynamic forces are contained within a module known as DYNARES. The primary functions of DYNARES are to assemble a model using the data previously described, to perform open- or closed-loop analyses of dynamic characteristics, and to provide reduced order plant design models for use in control law synthesis. Analyses performed with the model in the form of equations (1) and (2) can use the tabular aerodynamic data from DLAT or, alternatively, the rational function approximations thereof. Stability analyses using equations (1) and (2) are performed by the module STABCAR,[3] which is not directly connected to the data complex; but the DCM module can be used to provide an input data file for STABCAR.

The s-plane capabilities within DYNARES can be used to determine the rational function approximations to the frequency-dependent aerodynamic data using previously discussed Roger's or minimum-state approaches provided the denominator poles are chosen a priori. The data representing the resulting rational function approximations are stored on the data complex for use in forming a LTI state-space representation. Alternatively, a separate module, SPLFIT, can be employed to determine the column-independent, column-dependent, or minimum-state rational function approximations. This module also provides for optimization of the denominator pole locations.[5] The resulting data can be stored onto the data complex for subsequent use.

Sample Application Results

Results obtained with ISAC will now be presented that illustrate its utility in mathematical model development and in aeroelastic analyses.

Example Vehicle Description

The vehicle modeled and analyzed is an unpiloted drone, the DAST ARW-2 (drones for aerodynamic and structural testing, aeroelastic research wing number two)[20,21] shown in figure 4. All-moving stabilizers are identified and the locations of inboard and outboard ailerons are also indicated. A subset of the vehicle sensors and their locations are noted on the figure. The wing design and placement on the fuselage was such that flutter suppression, load alleviation, and rigid mode stability augmentation were required in regions of the vehicle flight envelope.

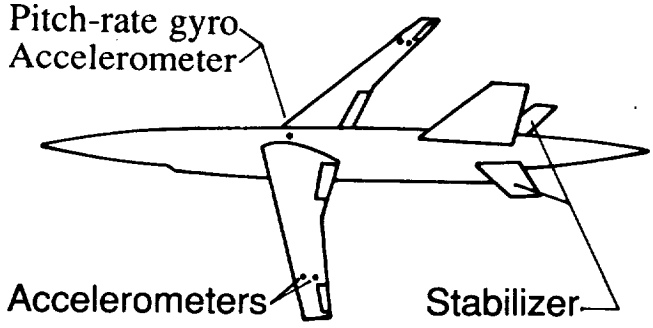

Fig. 4 Sketch of DAST ARW-2 vehicle.

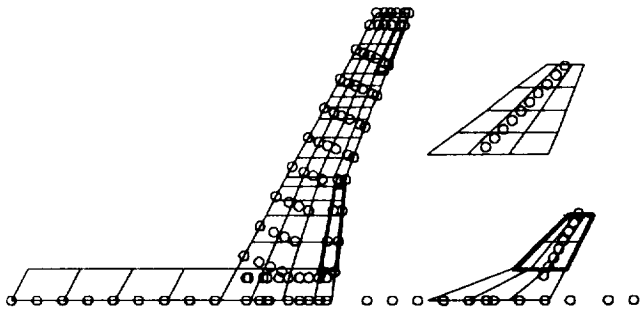

Fig. 5 Paneling and structural node information.

Inputs for Aerodynamic Force Computations

Figure 5 shows the planform views of the wing, horizontal tail, vertical tail, and a portion of the fuselage modeled as a lifting body. Alternatively, the fuselage could have been modeled as a slender body. For convenience, the vertical tail is shown in this view by translating it outboard and displaying its side view.

The boxes depict the elemental areas required for a doublet lattice representation of the lifting surfaces in terms of doublets on the one-quarter chord lines of each box. The boundaries of the control surfaces coincide with elemental box edges and are shown in the figure as darkened lines. There are no darkened lines on the vertical tail because it has no rudder.

The circles in figure 5 denote points at which modal data were available and indicate that the wing was modeled as a plate; whereas the fuselage and tails were modeled as beams. Twelve symmetric degrees of freedom were considered in the results to follow (plunge, pitch, and ten elastic modes) together with three control modes and one vertical gust input. At the mid span of each elemental box, displacement (at the one-quarter chord point) and displacement and slope (at the three-quarter chord point) are required for each generalized coordinate, control deflection and gust incidence angle in order to generate generalized aerodynamic forces corresponding to a particular Mach number and nondimensional frequency. Cubic splines in one (for beams) and two (for plates) dimensions[22] are used to perform the interpolations for modal deflections and slopes at the points required by the doublet lattice code. Examination of figure 5 and graphical display of modal deflection data, such as shown in figure 1, provide a valuable check for the correctness of the inputs into the DLAT module that are required for aerodynamic force generation prior to initiation of the computations.

Rational Function Approximations

Approximations of two elements of the unsteady aerodynamic force matrices are shown in figure 6 that were obtained using the Roger's option with $\ell_1 = 2$. The elements chosen are from the gust column, typically the column most difficult to fit. The figure provides a polar depiction of how the elements vary as a function of the (hidden) frequency variation; it compares the tabular data and the corresponding rational function approximations. The direction of increasing frequency is indicated on the figure. The approximation was constrained to fit the data precisely at zero frequency and to fit

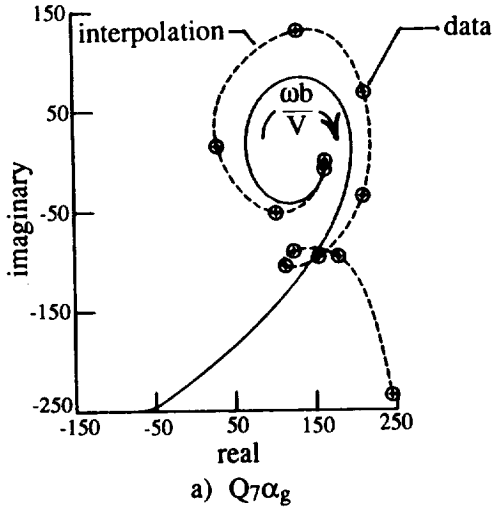

Fig. 6 Polar plots of generalized aero forces due to gust.

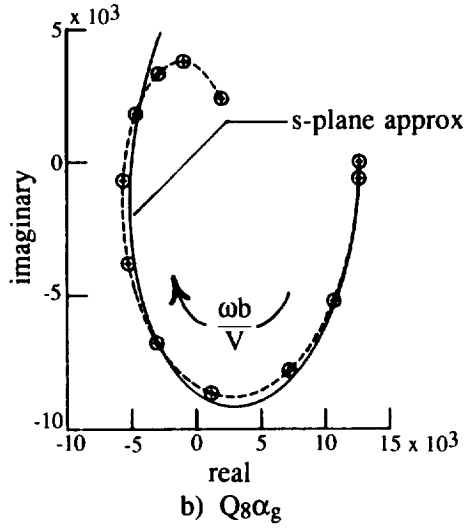

Fig. 6 Concluded.

the rate of change with respect to frequency at zero frequency. References 3 and 5 discuss the types of constraints that may be imposed in ISAC to ensure a good fit of the data in critical frequency regions.

Stability and Response Characteristics

Figure 7 shows the loci of the critical subset of elastic roots as a function of normalized controller feedback gain (the nominal gain has a magnitude of one) for a candidate single-input/single-output flutter suppression control law. Examination of the locus for the 4th mode reveals that the law does not achieve -6dB of gain margin. There are two curves for each root locus. These curves contrast the root loci obtained using the p-k approximation with root loci obtained using the rational function approximations for the unsteady aerodynamic forces. When these curves are generated using the iterative, Laplace-domain approach,[3] one can easily add a term in the controller transfer function corresponding to phase errors thereby exhibiting whether phase margin constraints are satisfied. For example, replace $T_C(s)$ with $\exp(i\pi/4)\, T_C(s)$ and repeat the analysis; if the system is stable at nominal gain, one has at least 45 degrees of margin to uniform phase errors in all inputs or in all outputs. Automated generation and graphical display of root loci are selectable within ISAC for feedback gain, density, altitude, and velocity variations under the assumption that Mach number is fixed.

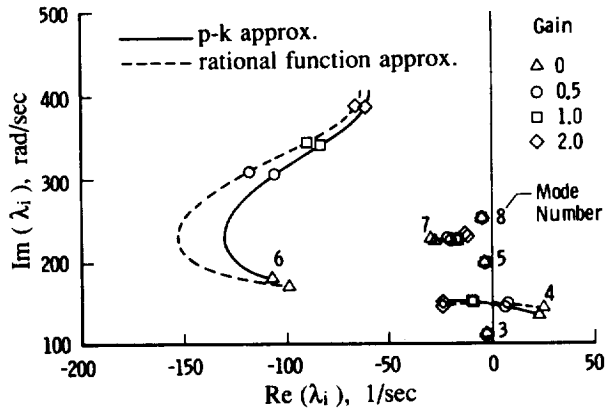

Fig. 7 Feedback gain loci of critical elastic roots.

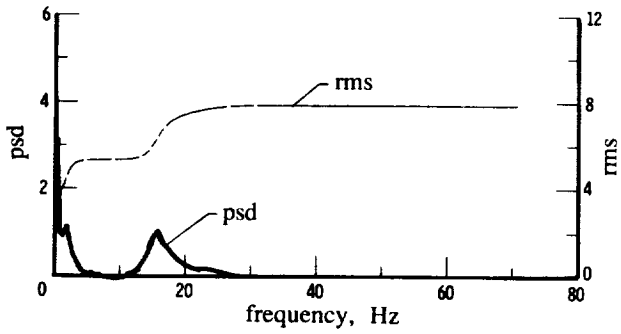

Fig. 8 Power spectral density of incremental wing root torsion.

An illustration of gust response analyses performed using the frequency-domain form of the equations is shown in figure 8. This analysis, valid only when the system (open- or closed- loop) is stable, shows the power spectral density (psd) of the incremental wing root torsion moment due to turbulence having the Von Karman spectrum. The psd shown has been normalized by lower dynamic pressure results. Also shown on the same figure is the cumulative rms of this load with frequency. These types of information can also be generated for other selectable outputs including control deflections and rates for Von Karman, Dryden, or user-defined rational polynomial definitions of turbulence spectra.

Reduced order approximations of mathematical models are often desirable in order to isolate the critical interactions, provide smaller, more manageable state-space models for control law design, or reduce the time required for analysis. Within ISAC, truncation and residualization options are available and are applied in the Laplace-domain representation (see equations (1) and (2)) as follows: Use the second block of rows of equation (1) to eliminate δ in the first block of rows; then partition ξ into low frequency, ξ_1, and stable, high frequency, ξ_2, modes yielding

$$\begin{bmatrix} G_{11}(s) & G_{12}(s) \\ G_{21}(s) & G_{22}(s) \end{bmatrix} \begin{pmatrix} \xi_1 \\ \xi_2 \end{pmatrix} = \begin{bmatrix} qQ_{\xi g}(s) & (qQ_{\xi\delta}(s)-M_{\xi\delta}s^2)T_\delta(s) \end{bmatrix} \begin{pmatrix} \alpha_g \\ u \end{pmatrix} = \begin{bmatrix} F_1(s) \\ F_2(s) \end{bmatrix} \begin{pmatrix} \alpha_g \\ u \end{pmatrix}. \quad (11)$$

Now retain only the static effects of ξ_2 by assuming ξ_2 reaches steady state instantaneously relative to ξ_1. Then

$$\begin{bmatrix} G_{11}(s) & G_{12}(0) \\ G_{21}(s) & G_{22}(0) \end{bmatrix} \begin{pmatrix} \tilde{\xi}_1 \\ \tilde{\xi}_2 \end{pmatrix} = \begin{bmatrix} F_1(s) \\ F_2(s) \end{bmatrix} \begin{pmatrix} \alpha_g \\ u \end{pmatrix} \quad (12)$$

can be used to eliminate $\tilde{\xi}_2$. The elimination is accomplished by solving for $\tilde{\xi}_2$ in terms of the other variables in the second block of rows of equation (12), substituting the result in the first block of rows, and collecting like terms. The result has the form

$$\tilde{G}_{11}(s)\tilde{\xi}_1 = \tilde{F}_1 \begin{pmatrix} \alpha_g \\ u \end{pmatrix} \quad (13)$$

and, by making the substitution for $\tilde{\xi}_2$ in equation (2), one can obtain

$$\tilde{y} = T_S(s)\,[\tilde{C}_1(s)\tilde{\xi}_1 + \tilde{C}_\delta(s)T_\delta(s)u + \tilde{C}_g(s)\alpha_g]. \quad (14)$$

If LTI state-space models (eqs. (6) and (7)) are created after residualization, model outputs are generated using eq. (2) with C_2 truncated, rather than eq. (14), which is an approximation if $C_2(s = 0) \neq 0$. Approximation can be avoided by performing residualization outside ISAC after generating a full-order state-space model.

Results are shown in figure 9 from a combined truncation and residualization model reduction at a flight condition well beyond flutter that was used as the primary active flutter suppression design point. Rigid body and essentially noninteracting elastic modes below the frequency of flutter (120 rad/sec) were removed by truncation. Modes of higher frequency that only had small impact upon the flutter mechanism were residualized. This figure exhibits magnitude of the frequency response of the difference between two accelerometer outputs due to a commanded trailing edge outboard control surface input ($u_{com_{teo}}$) for the full twelve mode model and for the five mode approximation. Good agreement is evident over a wide frequency range including the flutter frequency.

Figure 9 also serves to illustrate the capability for generation and display of frequency responses of interest. These frequency responses can then be used in design of control laws. When experimentally derived frequency responses are available over a portion of the desired frequency range, one can combine the experimental/analytical data to improve the representation of the plant.[18]

Time responses are computed within ISAC using the frequency-domain form of the equations coupled with Fourier transform techniques. An outline of the approach follows for a commanded input: Compute the fast Fourier transform (FFT), denoted by $\mathcal{F}$ in equation (15), of the input for a sample rate high enough to keep digital effects small in the frequency range of interest and to preclude aliasing within the user-controlled input frequency content.

$$u_{com_j}(\omega) = \mathcal{F}(u_{com_j}(t)). \quad (15)$$

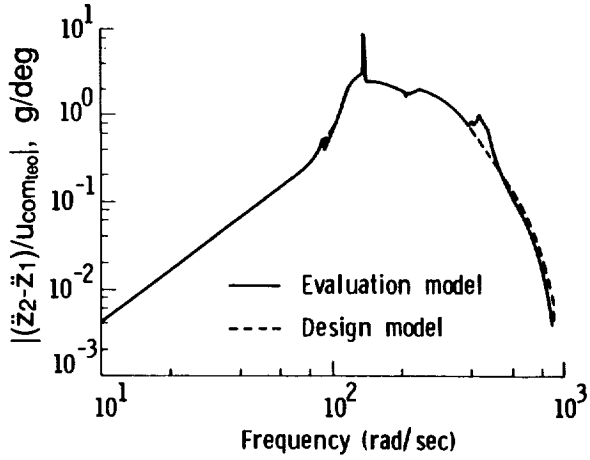

Fig. 9 Frequency response magnitudes.

The frequency and time variables are shown as bold to emphasize that there are a set of values of $u_{com_j}(\omega)$ and $u_{com_j}(t)$. Using equations (1), (2), and (3), compute the closed-loop frequency response, $\mathbf{H_j}(i\omega)$, of the outputs of interest. $\mathbf{H_j}(i\omega)$ need only be computed at a sufficient number of frequencies to allow accurate interpolation at frequencies corresponding to the FFT evaluation points where $u_{com_j}(\omega)$ is nonzero. Form the product

$$\mathbf{y}(\omega) = \mathbf{H_j}(i\omega)\, u_{com_j}(\omega)). \qquad (16)$$

Compute the inverse FFT of the outputs.

$$\mathbf{y}(t) = \mathcal{F}^{-1}(\mathbf{y}(\omega)). \qquad (17)$$

The time history generation process is illustrated in figures 10, 11, and 12 for symmetric input of a one-degree magnitude swept sine (sine chirp) command into each of the pair of trailing edge outboard control surface actuators ($u_{com_{teo}}$). Figure 10 shows the computed frequency response over the frequency range of the input. The commanded input is shown in figure 11 where the input frequency varies logarithmically with time from 5 Hz to 20 Hz over a 14.8 second time period. The amplitude of the input is ramped from zero to one degree maximum amplitude over a 0.05 second interval, ramped out near the end over the same interval of time, and followed with a short period of zero input. The output time history that results from the control input is shown in figure 12. The results are for an open-loop condition well below the flutter boundary. The composite sensor output is the difference of two outboard accelerometers located at approximately the same spanwise location (see figure 4). Consequently, the composite sensor output accentuates the observability of torsional motion. "Blossoming" of the accelerometer time response is evident as the input frequency passes through the frequency of one of the lightly damped poles that form the flutter mechanism at a higher frequency and at a higher dynamic pressure. Response is also seen at higher frequencies corresponding to other lowly damped elastic modes.

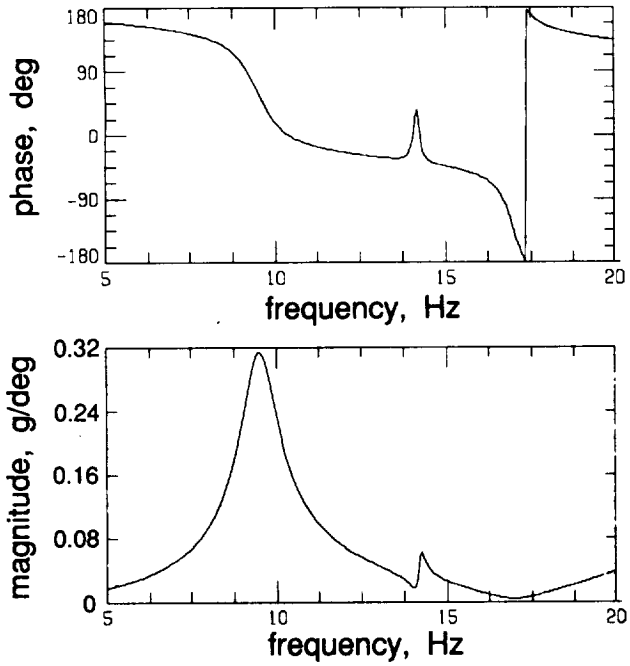

Fig. 10 Open-loop frequency response. $((\ddot{z}_2-\ddot{z}_1)/u_{com_{teo}})$

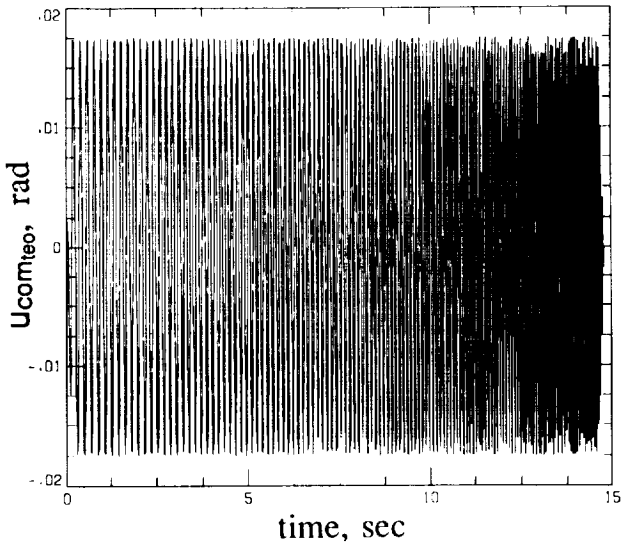

Fig. 11 Sine chirp command into outboard aileron actuator.

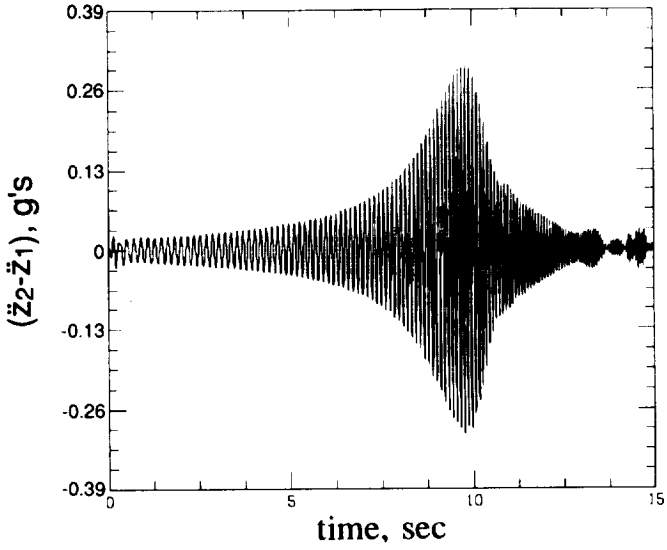

Fig. 12 $(\ddot{z}_2-\ddot{z}_1)$ due to sine chirp input into $u_{com_{teo}}$.

The majority of the graphical outputs that have been presented pertain to the frequency-domain representation of the model. The comparison of the s-plane approximation and the underlying numerically generated frequency-domain aerodynamic forces (figure 6) and the automated generation of the loci of roots with gain (figure 7), density, altitude, or velocity variation were examples of state-space related analysis capabilities within ISAC. The state-space option is primarily used for stability analyses and in the generation of plant models for use in control law design by other tools such as MATLAB[23] and MATRIX$_x$.[24] These external tools have capabilities that allow the generation of frequency and time responses of interest using the plant models.

ISAC Portability, Availability, and Documentation

ISAC is written in FORTRAN and will execute, with minimal changes relative to memory management, on many computer systems with a FORTRAN 77 compiler that supports namelist input. It is currently running on VAX micro II

computers with VMS, SUN Sparc workstations with a UNIX operating system (4.1 or greater), and IBM minicomputers. It is available through NASA with its own plotting package and library routines, and with preliminary versions of a user's manual and an extensive set of sample cases with documentation.

The ISAC system of programs has been or is currently being used in support of numerous projects such as:

- DAST ARW-1[25] and ARW-2[26]
- DC-10 wind tunnel flutter model[27]
- Generic X-wing feasibility studies[28]
- Analyses of elastic, oblique-wing aircraft[29]
- Active Flexible Wing (AFW) wind tunnel test program[18,30,31]
- Generic hypersonic vehicles[32,33]
- Benchmark active controls testing project
- High speed civil transport

There is a growing user community. The ISAC system has been transmitted, upon request, to a number of research facilities which includes:

- NASA Centers
  - Langley Research Center
    - Flight Systems Directorate
      - Guidance and Control Division
    - Structures Directorate
      - Structural Dynamics Division
  - Dryden Flight Research Facility
- United States Military
  - Department of the Air Force
    - AFWAL at Wright Patterson AFB
  - Department of the Navy
    - NADC at Warminster
- Companies
  - Lockheed Engineering and Sciences Company
  - Boeing Aircraft Company
  - McDonnell Douglas Aircraft Company
  - Learjet, Inc.
  - Leth and Associates
- Foreign Countries
  - Australia
    - Aeronautical Research Laboratories, Dept. of Defence
  - Canada
    - Aerodynamics/Dynamics of Flight Directorate, Canadian National Defence Headquarters, Institute for Aerospace Research
- Universities
  - Technion University (Israel)
  - Massachusetts Institute of Technology
  - University of Washington, Seattle
  - University of Florida

Concluding Remarks

An overview has been presented of the theoretical bases, aeroservoelastic modeling and analysis capabilities, and facilities for data storage and management for the ISAC system of program modules. Results are presented for a flexible aircraft that illustrate the major ISAC capabilities. References are cited which present research performed using ISAC for a variety of configurations. The results presented here and in the references demonstrate that ISAC is a useful tool for aeroservoelastic modeling and analysis.

ISAC is written in FORTRAN 77 and will execute, with minimal changes related to memory management, on many systems with a FORTRAN 77 compiler that supports namelist input. Preliminary versions of a user's manual and documentation containing an extensive set of sample cases are available.

Appendix: State-Space Equations in Flutter Axes

The plant state space matrices for the flutter axes choice of coordinate system and Roger's form (eq. (4)) of rational function approximations to the unsteady aerodynamic forces are more explicitly defined in this appendix.

$$[A \mid B] = \left[\begin{array}{c|c|c|c|c|c|c|c} 0 & I & 0 & 0 & 0 & 0 & 0 & 0 \\ \hline A_{\dot{\xi}\xi} & A_{\dot{\xi}\dot{\xi}} & A_{\dot{\xi}a} & 0 & A_{\dot{\xi}A} & A_{\dot{\xi}g} & B_{\dot{\xi}u} & B_{\dot{\xi}g} \\ \hline 0 & A_{a\dot{\xi}} & A_{aa} & 0 & A_{aA} & A_{ag} & 0 & B_{ag} \\ \hline A_{S\xi} & A_{S\dot{\xi}} & A_{Sa} & A_{SS} & A_{SA} & A_{Sg} & B_{Su} & B_{Sg} \\ \hline 0 & 0 & 0 & 0 & A_{AA} & 0 & B_{Au} & 0 \\ \hline 0 & 0 & 0 & 0 & 0 & A_{gg} & 0 & B_{gg} \end{array}\right]$$

$$A_{\dot{\xi}\xi} = -\mathcal{M}^{-1}\mathcal{K} = -\mathcal{M}^{-1}\left(K_{\xi\xi} - qA_0^{\xi}\right),$$

$$\mathcal{M} = M_{\xi\xi} - q\left(\frac{b}{V}\right)^2 A_2^{\xi}.$$

$$A_{\dot{\xi}\dot{\xi}} = -\mathcal{M}^{-1}\mathcal{D} = -\mathcal{M}^{-1}\left(D_{\xi\xi} - q\frac{b}{V}A_1^{\xi}\right).$$

See equation (4) for the A_i. The matrix $D_{\xi\xi}$ is diagonal and viscous in form; the ith diagonal term is

$$D_{\xi_i\xi_i} = g_{s_i} m_{\xi_i\xi_i} \omega_{n_i}.$$

Refer to the expansion of terms below equation (1) for definition of the variables.

$$A_{\dot{\xi}a} = q\mathcal{M}^{-1}\begin{bmatrix} 11\cdots1 & 0 & \cdots & \cdots & 0 \\ 0 & 11\cdots1 & 0 & \cdots & \vdots \\ \vdots & 0 & \ddots & \ddots & \vdots \\ \vdots & \vdots & \ddots & \ddots & 0 \\ 0 & 0 & \cdots & 0 & 11\cdots1 \end{bmatrix},$$

where each of the n_ξ rows contains ℓ_1 ones in the indicated columns. The aerodynamic states are ordered such that the effects of all lags upon each particular generalized coordinate are grouped together.

$$A_{\dot{\xi}A} = -\mathcal{M}^{-1}\left[\mathcal{K}_\delta \quad \mathcal{D}_\delta \quad \mathcal{M}_\delta\right]\begin{bmatrix} C_A \\ C_{A_1} \\ C_{A_2} \end{bmatrix},$$

where

$$\mathcal{K}_\delta = -qA_0^\delta, \quad \mathcal{D}_\delta = -q\frac{b}{V}A_1^\delta, \quad \mathcal{M}_\delta = M_{\xi\delta} - q\left(\frac{b}{V}\right)^2 A_2^\delta.$$

See the discussion of the actuator state rows below for a definition of C_A, C_{A_1}, and C_{A_2}.

$$A_{\dot{\xi}g} = \mathcal{M}^{-1}\left[\frac{q}{V}A_0^g \;\middle|\; \frac{q}{V}\frac{b}{V}A_1^g\right]\begin{bmatrix} C_g \\ \hline C_{\dot{g}1} \end{bmatrix},$$

where the dynamic element whose output has the desired gust

velocity spectrum is required to have a denominator polynomial of order at least one greater than its numerator polynomial. The constraint $\mathbf{A}_2^g = \mathbf{0}$ is also imposed. For the Dryden vertical gust spectrum

$$\dot{\mathbf{x}}_g = \mathbf{A}_g\mathbf{x}_g + \mathbf{B}_g\eta, \quad w_g = \mathbf{C}_g\mathbf{x}_g, \quad \mathbf{C}_g = \left[1 \;\middle|\; \frac{\sqrt{3}g_L}{V}\right],$$

$$\mathbf{A}_g = \left[\begin{array}{c|c} 0 & 1 \\ \hline -\left(\frac{V}{g_L}\right)^2 & -\frac{2V}{g_L} \end{array}\right], \quad \mathbf{B}_g = \left[\begin{array}{c} 0 \\ \hline \sqrt{\left(\frac{V}{g_L}\right)^3}\sigma_{w_g} \end{array}\right]$$

$$\mathbf{C}_{g1} = \left[-\frac{\sqrt{3}V}{g_L} \;\middle|\; 1-2\sqrt{3}\right], \quad \mathbf{D}_{g1} = \sqrt{\frac{3V}{g_L}}\sigma_{w_g},$$

where g_L is a gust reference length and σ_{w_g} is rms gust velocity.

$$\mathbf{B}_{\dot{\xi}u} = -\mathcal{M}^{-1}\mathcal{M}_\delta\mathbf{D}_{A_2}, \quad \mathbf{B}_{\dot{\xi}g} = \mathcal{M}^{-1}\frac{q}{V}\frac{b}{V}\mathbf{A}_1^g\mathbf{D}_{g1},$$

$$\left[\mathbf{A}_{a\dot{\xi}} \;\middle|\; \mathbf{A}_{aA} \;\middle|\; \mathbf{A}_{ag} \;\middle|\; \mathbf{B}_{ag}\right] =$$

$$\left[\begin{array}{c|c|c|c} {}^1\mathbf{A}^\xi & \left({}^1\mathbf{A}^\delta\right)\mathbf{C}_{A_1} & \frac{1}{V}\left({}^1\mathbf{A}^g\right)\mathbf{C}_{g1} & \frac{1}{V}\left({}^1\mathbf{A}^g\right)\mathbf{D}_{g1} \\ \hline \vdots & \vdots & \vdots & \vdots \\ \hline {}^{n_\xi}\mathbf{A}^\xi & \left({}^{n_\xi}\mathbf{A}^\delta\right)\mathbf{C}_{A_1} & \frac{1}{V}\left({}^{n_\xi}\mathbf{A}^g\right)\mathbf{C}_{g1} & \frac{1}{V}\left({}^{n_\xi}\mathbf{A}^g\right)\mathbf{D}_{g1} \end{array}\right],$$

where

$${}^i\mathbf{A} = \left[\begin{array}{c} \text{ith row of } \mathbf{A}_3 \\ \hline \text{ith row of } \mathbf{A}_4 \\ \hline \vdots \\ \hline \text{ith row of } \mathbf{A}_{\ell_1+2} \end{array}\right].$$

$$\mathbf{A}_{aa} = -\frac{V}{b}\left[\begin{array}{ccc|ccc} b_1 & & & & & \\ b_2 & \ddots & & & & \\ & & b_{\ell_1} & & & \\ \hline & & & b_1 & & \\ & & & b_2 & \ddots & \\ & & & & & b_{\ell_1} \end{array}\right],$$

where there are n_ξ repetitions of the set of lag coefficients.

The input into the sensors (output from the plant) has the form

$$\mathbf{y}_p = \mathbf{C}_{pp}^A\ddot{\xi} + \mathbf{C}_{p\delta}^A\ddot{\delta} + \mathbf{C}_{pp}^R\dot{\xi} + \mathbf{C}_{p\delta}^R\dot{\delta} + \mathbf{C}_{pg}^R\frac{w_g}{V} + \mathbf{C}_{pp}^D\xi + \mathbf{C}_{p\delta}^D\delta.$$

The A refers to acceleration, the R to rate, and the D to displacement. The matrix coefficients with δ in the subscript are zero unless the sensors are on a control surface. The matrix with the g subscript allows inclusion of a gust vane sensor.

The vector, $\mathbf{y}_p$, provides the inputs to the following sensor dynamics equations:

$$\dot{\mathbf{x}}_S = \mathbf{A}_S\mathbf{x}_S + \mathbf{B}_S\mathbf{y}_p, \qquad \mathbf{y}_S = \mathbf{C}_S\mathbf{x}_S + \mathbf{D}_S\mathbf{y}_p.$$

The sensor system matrix is block diagonal with one block for each sensor. Currently, the system matrix for each sensor is expressed in numerically nonoptimum controller canonical form. The matrices in the sensor dynamics states rows are

$$\mathbf{A}_{S\xi} = \mathbf{B}_S(\mathbf{C}_{pp}^A\mathbf{A}_{\dot{\xi}\xi} + \mathbf{C}_{pp}^D), \qquad \mathbf{A}_{S\dot{\xi}} = \mathbf{B}_S(\mathbf{C}_{pp}^A\mathbf{A}_{\dot{\xi}\dot{\xi}} + \mathbf{C}_{pp}^R),$$

$$\mathbf{A}_{Sa} = \mathbf{B}_S\mathbf{C}_{pp}^A\mathbf{A}_{\dot{\xi}a}, \qquad \mathbf{A}_{SS} = \mathbf{A}_S,$$

$$\mathbf{A}_{SA} = \mathbf{B}_S(\mathbf{C}_{pp}^A\mathbf{A}_{\dot{\xi}A} + \mathbf{C}_{p\delta}^A\mathbf{C}_{A_2} + \mathbf{C}_{p\delta}^R\mathbf{C}_{A_1} + \mathbf{C}_{p\delta}^D\mathbf{C}_A),$$

$$\mathbf{A}_{Sg} = \mathbf{B}_S(\mathbf{C}_{pp}^A\mathbf{A}_{\dot{\xi}g} + \mathbf{C}_{pg}^R\frac{\mathbf{C}_g}{V}),$$

$$\mathbf{B}_{Su} = \mathbf{B}_S(\mathbf{C}_{pp}^A\mathbf{B}_{\dot{\xi}u} + \mathbf{C}_{p\delta}^A\mathbf{D}_{A_2}), \qquad \mathbf{B}_{Sg} = \mathbf{B}_S\mathbf{C}_{pp}^A\mathbf{B}_{\dot{\xi}g}.$$

See the next paragraph for definition of $\mathbf{D}_{A_2}$.

The actuator state equations have block diagonal system matrices with each block representing one actuator in controller canonical form. It is required that each actuator transfer function have denominator polynomial at least two orders higher than its numerator. The following equations result:

$$\dot{\mathbf{x}}_A = \mathbf{A}_A\mathbf{x}_A + \mathbf{B}_A\mathbf{u}, \qquad \delta = \mathbf{C}_A\mathbf{x}_A,$$

$$\dot{\delta} = \mathbf{C}_A\dot{\mathbf{x}}_A = \mathbf{C}_A\mathbf{A}_A\mathbf{x}_A = \mathbf{C}_{A_1}\mathbf{x}_A,$$

$$\ddot{\delta} = \mathbf{C}_{A_1}\dot{\mathbf{x}}_A = \mathbf{C}_{A_1}(\mathbf{A}_A\mathbf{x}_A + \mathbf{B}_A\mathbf{u}) = \mathbf{C}_{A_2}\mathbf{x}_A + \mathbf{D}_{A_2}\mathbf{u},$$

$$\mathbf{A}_{AA} = \mathbf{A}_A, \qquad \mathbf{B}_{Au} = \mathbf{B}_A.$$

The gust state-space equations, defined previously, introduce the following matrices in the plant state-space equations:

$$\mathbf{A}_{gg} = \mathbf{A}_g, \qquad \mathbf{B}_{gg} = \mathbf{B}_g.$$

The following vector of output equations is generated in the state-space representation:

$$\mathbf{y}^T = \left[\mathbf{y}_p^T, \mathbf{u}_{com}^T, \mathbf{y}_S^T, (\mathbf{u}-\mathbf{u}_{com})^T, \delta^T, \dot{\delta}^T, \ddot{\delta}^T, \mathbf{L}^T, \frac{\mathbf{w}_g^T}{V}\right].$$

The vector $\mathbf{L}$ is a modal displacement characterization of incremental loads wherein

$$\mathbf{L} = \mathbf{C}_\xi\xi.$$

The equations presented in the body of the text and in this appendix are sufficient to define the system matrices $\mathbf{C}$, $\mathbf{D}_u$ and $\mathbf{D}_g$ of equation (7).

References

1. Peele, E. L.; and Adams, W. M., Jr.: "A Digital Program for Calculating the Interaction Between Flexible Structures, Unsteady Aerodynamics, and Active Controls," NASA TM-80040, Jan. 1979.
2. Adams, William M., Jr.; Tiffany, Sherwood H.; and Newsom, Jerry R.: "Tools for Active Control System Design," *Presented at the 1st Annual NASA Aircraft Controls Workshop*, Hampton, VA. NASA CP-2296, pp. 263-280, October 25-27, 1983.
3. Adams, W. M., Jr.; Tiffany, S. H.; Newsom, J. R.; and Peele, E. L.: "STABCAR---A Program for Finding Characteristic Roots of Systems Having Transcendental Stability Matrices," NASA TP-2165, June 1984.
4. Newsom, J. R.; Adams, W. M., Jr.; Abel, I.; Tiffany, S. H.; and Mukhopadhyay, V.: "Active Controls: A Look at Analytical Methods and Associated Tools." *Presented at the 14th ICAS Congress*, Toulouse, France. September 9-14, 1984.
5. Tiffany, Sherwood H.; and Adams, William M., Jr.: "Nonlinear Programming Extensions to Rational Function Approximation Methods for Unsteady Aerodynamic Forces." NASA TP-2776, July 1988.
6. Tinoco, E. N.; and Mercer, J. E.: "FLEXSTAB--A Summary of the Functions and Capabilities of the NASA Flexible Airplane Analysis Computer System." NASA CR 2564, October 1974.
7. Rodden, William P.; Harder, Robert L.; and Bellinger, E. Dean: "Aeroelastic Addition to NASTRAN." NASA CR-3146, 1979.
8. Perry, B. III; Kroll, R. I.; Miller, R. D.; and Goetz, R. C.: "DYLOFLEX: A Computer Program for Flexible Aircraft Flight Dynamic Loads Analysis with Active Controls." *Journal of Aircraft*, vol. 17, no. 4, Apr. 1980, pp. 275-282.
9. Noll, T.; Blair, M.; and Cerra, J.: "ADAM, an Aeroservoelastic Analysis Method for Analog or Digital Systems." *Journal of Aircraft*, Nov. 1986.
10. Gupta, K. K.; Brenner, M. J.; and Voelker, L. S.: "Development of an Integrated Aeroservoelastic Analysis Program and Correlation with Test Data." NASA TP-3120, 1991.
11. Hassig, Hermann J.: "An Approximate True Damping Solution of the Flutter Equation by Determinant Iteration." *Journal of Aircraft*, vol. 8, no. 11, Nov. 1971, pp. 885-889.
12. Oppenheim, Alan V.; and Schafer, Ronald W.: *Discrete Time Signal Processing*. Prentice-Hall, 1989, Englewood Cliffs, NJ 07632.
13. Roger, Kenneth L.: "Airplane Math Modeling Methods for Active Control Design." *Structural Aspects of Active Controls*, AGARD-CP-228, Aug. 1977, pp. 4-1 to 4-11.
14. Vepa, Ranjan: "Finite State Modeling of Aeroelastic Systems." NASA CR-2779, 1977.
15. Edwards, John William: "Unsteady Aerodynamic Modeling and Active Aeroelastic Control." SUDAAR 504 (NASA Grant NGL-05-020-007), Dept. of Aeronautics and Astronautics, Stanford Univ., Feb 1977. (Available as NASA CR-148019).
16. Karpel, Mordechay: "Design for Active and Passive Flutter Suppression and Gust Alleviation." NASA CR-3482, 1981.
17. Dunn, H. J.: "An Analytical Technique for Approximating Unsteady Aerodynamics in the Time Domain." NASA TP-1738, 1980.
18. Christhilf, David M.; and Adams, William M., Jr.: "Multifunction Tests of a Frequency Domain Based Flutter Suppression System." NASA TM-107617, May 1992.
19. Giesing, J. P.; Kalman, T. P.; and Rodden, W. P.: "Subsonic Unsteady Aerodynamics for General Configurations. Part I, Volume I--Direct Application of the Nonplanar Doublet-Lattice Method." AFFDL-TR-71-5, Pt.I, Vol. I, U. S. Air Force, Nov. 1971 (Available from DTIC as AD 891 403L).
20. Boeing Wichita Company: "Integrated Design of a High Aspect Ratio Research Wing with an Active Control System for Flight Tests on a BQM-34E/F Drone Vehicle." NASA CR 166108, 1979.
21. Boeing Wichita Company: "Integrated Design of a High Aspect Ratio Research Wing with an Active Control System for Flight Tests on a BQM-34E/F Drone Vehicle." NASA CR 166109, 1979.
22. Harder, Robert L.; and Desmarias, Robert N.: "Interpolation Using Surface Splines." *Journal of Aircraft*, vol. 9, no. 2, Feb. 1972, pp. 189-191.
23. *PRO-MATLAB User's Guide*. The Mathworks Inc., Cochituate Place, 24 Prime Park Way, Natick, MA 01760.
24. Walker, Robert; Gregory, Charles, Jr.; and Shah, Sunil: "MATRIX$_X$: A Data Analysis, System Identification, Control Design, and Simulation Package." *Control System Magazine*, vol. 2, no. 4, Dec. 1982, pp. 30-37.
25. Newsom, Jerry R.; Pototzky, Anthony S.; and Abel, Irving: "Design of the Flutter Suppression System for DAST ARW-1R - A Status Report." NASA TM 84642, May 1983.
26. Adams, William M. Jr.; and Tiffany, Sherwood H.: "Design of a Candidate Flutter Suppression Control Law for DAST ARW-2." NASA TM-86257, July 1984.
27. Abel, Irving; Perry, Boyd, III; and Newsom, Jerry R.: "Comparison of Analytical and Wind-Tunnel Results for Flutter and Gust Response of a Transport Wing with Active Controls." NASA TP 2010, June 1982.
28. Woods, J. A.; Gilbert, M. G.; and Weisshaar, T. A.: "Parametric Aeroelastic Stability Analysis of a Generic X-Wing Aircraft." *Journal of Aircraft*, vol. 27, no. 7, July 1990, pp. 653-659.
29. Burken, John J.; Alag, Gurbux S.; and Gilyard, Glenn B.: "Aeroelastic Control of Oblique-Wing Aircraft." NASA TM-86808, 1986.
30. Buttrill, C. S.; Houck, J. A.; and Heeg, J.: "Hot Bench Simulation of the Active Flexible Wing Wind-Tunnel Model." AIAA Paper 90-3121, *Proceedings of Flight Simulation Technologies Conference*, AIAA, Dayton, OH. Sept. 1990.
31. Buttrill, C. S.; Bacon, B. J.; Heeg, J.; Houck, J. A.; and Wood, D.: "Simulation and Model Reduction for the AFW Program." AIAA Paper 92-2081, *Proceedings of the Dynamics Specialists Conference*, AIAA, Dallas TX. Apr. 1992.
32. Raney, David L.; Pototzky, Anthony S.; McMinn, John D.; and Wooley, Christine L.: "Impact of Aero-Propulsive-Elastic Interactions on Longitudinal Flight Dynamics of an Air-Breathing Hypersonic Vehicle." AIAA Paper No. 93-1367, *Proceedings of the 34th Structures, Structural Dynamics, and Materials Conference*, AIAA, La Jolla, CA, Apr. 19-22, 1993.
33. Spain, Charles V.; Zeiler, Thomas A.; Gibbons, Michael D.; Soistmann, David L.; Pozefsky, Peter; DeJesus, Rafael O.; and Brannon, Cyprian P.: "Aeroelastic Character of a National Aerospace Plane Demonstrator Concept." AIAA Paper No. 93-1314, *Proceedings of the 34th Structures, Structural Dynamics, and Materials Conference*, AIAA, La Jolla, CA, Apr. 19-22, 1993.

REPORT DOCUMENTATION PAGE

Form Approved
OMB No. 0704-0188

1. AGENCY USE ONLY *(Leave blank)*	2. REPORT DATE	3. REPORT TYPE AND DATES COVERED
	December 1993	Technical Memorandum

4. TITLE AND SUBTITLE
ISAC: A Tool for Aeroservoelastic Modeling and Analysis

5. FUNDING NUMBERS
505-64-52-03

6. AUTHOR(S)
William M. Adams, Jr. and Sherwood T. Hoadley

7. PERFORMING ORGANIZATION NAME(S) AND ADDRESS(ES)
NASA Langley Research Center
Hampton, VA 23681-0001

8. PERFORMING ORGANIZATION REPORT NUMBER

9. SPONSORING / MONITORING AGENCY NAME(S) AND ADDRESS(ES)
National Aeronautics and Space Administration
Washington, DC 20546-0001

10. SPONSORING / MONITORING AGENCY REPORT NUMBER
NASA TM-109031

11. SUPPLEMENTARY NOTES

12a. DISTRIBUTION / AVAILABILITY STATEMENT
Unclassified - unlimited

Subject Categories - 08,61

12b. DISTRIBUTION CODE

13. ABSTRACT *(Maximum 200 words)*

This paper discusses the capabilities of the Interaction of Structures, Aerodynamics, and Controls (ISAC) system of program modules. The major modeling, analysis, and data management components of ISAC are identified. Equations of motion are displayed for a Laplace-domain representation of the unsteady aerodynamic forces. Options for approximating a frequency-domain representation of unsteady aerodynamic forces with rational functions of the Laplace variable are shown. Linear time invariant state-space equations of motion that result are discussed. Model generation and analyses of stability and dynamic response characteristics are shown for an aeroelastic vehicle which illustrate some of the capabilities of ISAC as a modeling and analysis tool for aeroelastic applications.

14. SUBJECT TERMS	15. NUMBER OF PAGES
Aeroservoelasticity, linear modeling and analysis, active controls, stability, deterministic and stochastic response, and ISAC	11
	16. PRICE CODE: A03

17. SECURITY CLASSIFICATION OF REPORT	18. SECURITY CLASSIFICATION OF THIS PAGE	19. SECURITY CLASSIFICATION OF ABSTRACT	20. LIMITATION OF ABSTRACT
unclassified	unclassified	unclassified	

NSN 7540-01-280-5500

Standard Form 298 (Rev. 2-89)
Prescribed by ANSI Std. Z39-18
298-102